



53424

AIAA 93-3519
Full-Scale Wind Tunnel Studies
of F/A-18 Tail Buffet

Larry A. Meyn
NASA Ames Research Center, Moffett Field, CA

Kevin D. James
Sterling Federal Systems, Inc., Palo Alto, CA

AIAA Applied Aerodynamics
Conference

August 9-11, 1993 / Monterey, CA

Full-Scale Wind Tunnel Studies of F/A-18 Tail Buffet

Larry A. Meyn*

NASA Ames Research Center, Moffett Field, California 94035

and

Kevin D. James†

Sterling Federal Systems, Inc., Palo Alto, California 94303

ABSTRACT

Tail buffet studies were conducted on a full-scale, production, F/A-18, fighter aircraft in the 80- by 120-Foot Wind Tunnel of the National Full-Scale Aerodynamic Complex at NASA Ames Research Center in Moffett Field, California. The F/A-18 was tested over an angle-of-attack range of 18° to 50° , a side-slip range of -15° to 15° , and at wind speeds of up to 100 knots. The maximum speed corresponds to a Reynolds number of 12.3×10^6 based on mean aerodynamic chord and a Mach number of 0.15. The port, vertical tail fin was instrumented with thirty-two surface pressure transducers, arranged in four by four arrays on both sides on the fin. The aircraft was also equipped with a removable Leading Edge eXtension (LEX) fence that is used on F/A-18 aircraft to reduce tail buffet loads. Time-averaged, power-spectral analysis results are presented for the tail fin bending moment derived from the integrated pressure field. The results are only for the zero side-slip condition, both with and without the LEX fence. The LEX fence significantly reduces the magnitude of the root-mean-square pressures and bending moments. Scaling issues are addressed by comparing full-scale results for pressures at the 60%-span and 45%-chord location with published results of small-scale, F/A-18 tail-buffet tests. The comparison shows that the tail buffet frequency scales very well with length and velocity. Root-mean-square pressures and power spectra do not scale as well. The LEX fence is shown to reduce tail buffet loads at all model scales.

NOMENCLATURE

\bar{c}	mean aerodynamic chord (m.a.c.), 11.52 ft
$Re_{\bar{c}}$	Reynolds number based on m.a.c.
α	angle-of-attack, degrees
b	reference wing span, 37.42 ft
$C_{p''}$	pressure power coefficient, $\frac{4p''}{\rho^2 V^3}$
$C_{p'}$	RMS pressure coefficient, $\frac{p'}{\frac{1}{2}\rho V^2}$
F	reduced frequency, l/fV

f	frequency, Hz
l	characteristic length, 11.52 ft
p''	pressure power, psi^2/Hz
p'	RMS pressure, psi
q_∞	free-stream dynamic pressure, $\frac{1}{2}\rho V^2$, psf
ρ	density, 0.00237 slugs/ft ³
S	reference wing area, 400 ft ²
V	velocity, ft/sec

INTRODUCTION

Tail buffet occurs when the vortex shed from a strake or a LEX bursts immediately forward of the tail. Although tail buffet can be a problem for any aircraft, it is a special concern for twin-tailed fighter aircraft. The F/A-18, in particular, had serious fatigue problems due to tail buffeting until a vertical plate, referred to as the LEX fence, was developed and installed on the aircraft, Fig. 1. To show the effect of the LEX fence on tail buffeting, this paper presents tail buffet data for the aircraft at zero sideslip, both with and without the LEX fence. Several studies of F-18 tail buffeting have also been carried out in small-scale tests¹⁻⁵ and in numerical simulations^{6,7}.

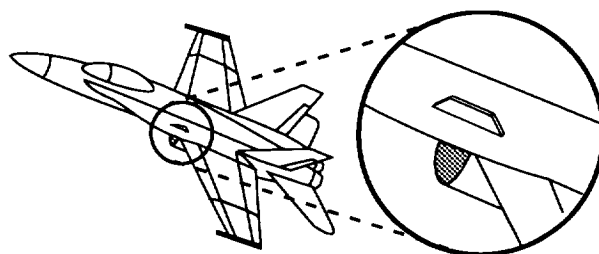


Fig. 1 F/A-18 LEX Fence

The first full-scale F/A-18 wind tunnel test, Fig. 2, was conducted as part of NASA's High Alpha Technology Program (HATP). The objective of the HATP program is to provide new technology and to validate design methods for the next generation of highly maneuverable aircraft. The HATP program encompasses several research efforts within NASA that include small-scale wind tunnel and water tunnel tests, flight tests with the High Angle-of-Attack Research Vehicle (HARV), CFD computations, and the full-scale wind tunnel tests conducted in the 80- by 120-Foot Wind Tunnel. In addition to the tail buffet studies, the full-scale F/A-18 wind tunnel tests include studies of forebody vortex control devices, CFD validation studies, and the compilation of surface pressure and force data to compare to small-scale tests and to flight. These studies will continue in future tests of the F/A-18 in the 80- by 120-Foot Wind Tunnel. A survey of the results obtained in

* Aerospace Engineer. Member AIAA.

† Aerospace Engineer. Member AIAA.

Copyright © 1993 by the American Institute of Aeronautics and Astronautics, Inc. No copyright is asserted in the United States under Title 17, U.S. Code. The U.S. Government has a royalty-free license to exercise all rights under the copyright claimed herein for Governmental purposes. All other rights are reserved by the copyright owner.

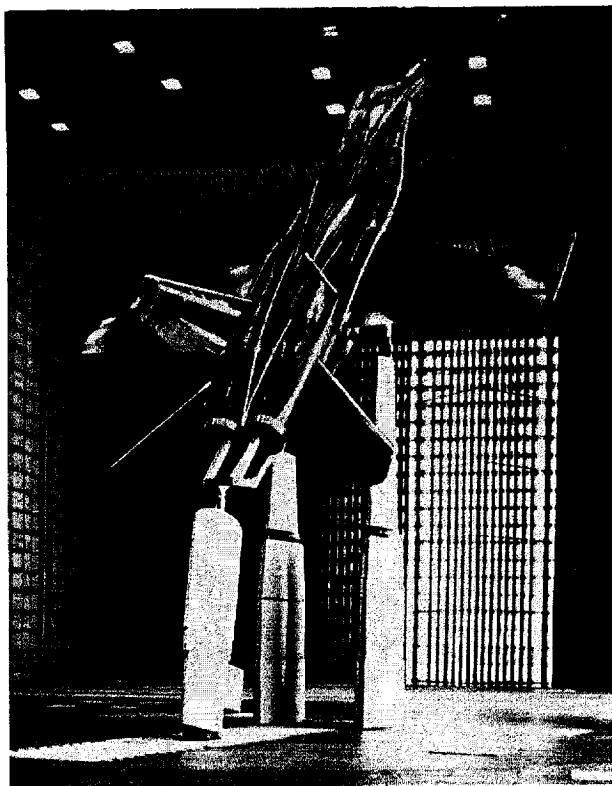


Fig. 2 The F/A-18 in the 80- by 120-Foot Wind Tunnel.

the first full-scale F/A-18 wind tunnel test is given in reference 8.

The three principle objectives of the full-scale tail buffet tests are: 1) to study the flow field characteristics of tail buffet over a wide range of angle-of-attack and sideslip, 2) to quantify the effects the LEX fence in reducing tail buffet loads, and 3) to provide full-scale data to compare with data obtained in small-scale wind tunnels. The goal of the first objective is to understand how angle-of-attack and sideslip affect tail buffet loads on twin-tailed aircraft. The data obtained will also be used to determine tail loading conditions for full-scale structural fatigue tests of the F/A-18.² The goal of the second objective is to understand why the LEX fence reduces tail buffet loads. This information could lead to the development of alternative methods to reduce tail buffet loads. Finally, the goal of the last objective is to aid in the development of guidelines to quantitatively predict tail buffet loads in flight from small-scale wind tunnel data. To address this objective, pressure transducers were located on the full-scale aircraft in many of the same locations used in small-scale tests, allowing direct comparisons of full-scale data with data obtained at small-scale. Several comparisons of full-scale data with published small-scale data are presented in this paper.

EXPERIMENTAL SETUP

Wind Tunnel

The 80- by 120-Foot Wind Tunnel is part of the National Full-Scale Aerodynamic Complex (NFAC) located at NASA Ames Research Center⁹. The NFAC

can be configured as either a closed circuit wind tunnel with a 40- by 80-foot test section or an open circuit wind tunnel with an 80- by 120-foot test section. A schematic of the facility is shown in Fig. 3. The maximum dynamic pressure attainable in the 80- by 120-Foot Wind Tunnel is 33 psf, providing a maximum velocity of approximately 100 knots. The wind tunnel is driven by six 40 foot diameter, variable speed, variable pitch fans. Each fan is powered by a 22500 hp electric motor and at full speed the wind tunnel draws 106 MW of power.

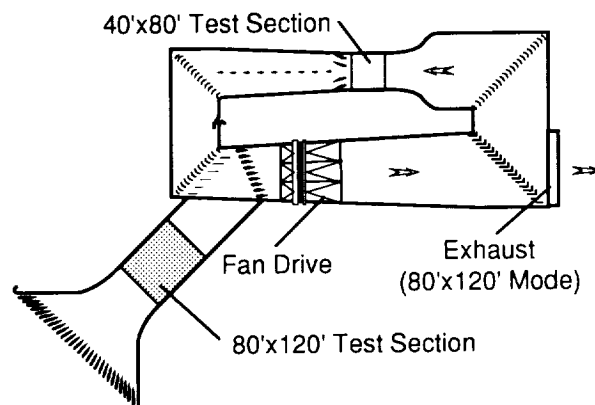


Fig. 3 Schematic of the National Full-Scale Aerodynamic Complex.

The aircraft was supported in the wind tunnel test section by the three struts shown in Figs. 2 and 4. The two, fixed height, main struts were connected by a horizontal cross-bar. The aircraft was attached to the cross-bar with two blade and clevis assemblies that replaced the main landing gear trunnions. The tail strut is a large linear actuator that pitches the aircraft about main strut attachment pivots. In order to maintain a positive mechanical advantage at higher angles of attack, it was necessary to attach the tail strut to a point aft of the aircraft. This was achieved with a cantilevered structure connected to the F/A-18 engine mounts and to the arresting hook pivot, Figs. 2 and 4.

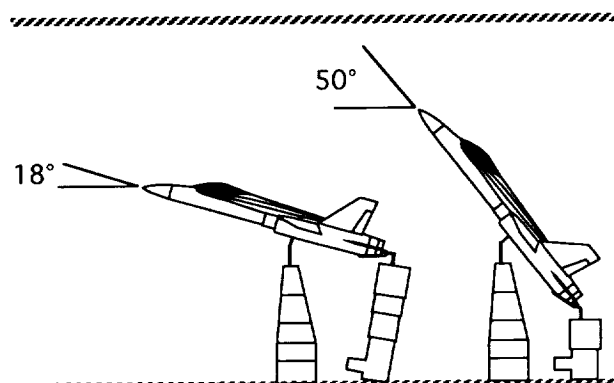


Fig. 4 Aircraft on struts for minimum and maximum angle of attack.

The three struts are mounted on a rotatable turntable that is supported by a six-component scale system. Each strut has a non-metric aerodynamic fairing mounted on a non-metric turntable that tracks the balance turntable.

The fairings rotate to stay aligned with the wind tunnel axis when the turn table rotates to yaw the aircraft. The fairing for the tail strut changes length and tilt angle to follow the tail strut when the aircraft is pitched.

Test Article

The aircraft, supplied by the U.S. Navy, is from the first F/A-18 model A production block. The aircraft engines and avionics were removed prior to shipment to Ames Research Center. The aircraft is 56.0 ft long, has a wing span of 37.42 ft, the reference wing area is 400 ft², and the mean aerodynamic chord is 11.52 ft. Figure 4 is a schematic showing the aircraft in the 80 ft high test section at the minimum and maximum angles of attack for this test. The aircraft was mounted slightly below the centerline of the test section to reduce the effect of ceiling proximity on the forebody at high angles-of-attack. Wind tunnel blockage at 20° angle-of-attack is slightly less than 4.9% and climbs to less than 7.5% for an angle-of-attack of 50°.

The aircraft was configured with flow-through inlets. The aircraft missile rails were left in place, however, no missiles were attached. The aircraft had removable LEX Fences, Fig. 1, which are installed on all U.S. Navy F/A-18 aircraft to reduce tail buffet loads. The LEXs used in this test were the pressure instrumented pair normally flown on the HARV. The LEX fences are trapezoidal in shape, 8.375 inches high, 36.6 inches long at the base, and 27.9 inches long at the top.

The leading-edge flaps were fixed at a 33° deflection angle and trailing-edge flaps were fixed in their undeflected position. These flap deflections match the standard control-law schedule for angles-of-attack greater than 26°. The rudders were fixed in their undeflected position. The horizontal stabilators were actuated and their position was varied with angle-of-attack to match the trimmed stabilator positions of the HARV in steady, 1 "g" flight conditions.

Instrumentation

The tail buffet instrumentation consisted of thirty-two 15 psia pressure transducers, eight accelerometers, six strain gages, and a surface temperature sensor. The pressure transducers were mounted on the surface of the left vertical tail in a four by four matrix on both the inboard and outboard surfaces, Fig. 5. Each vertical tail and each horizontal stabilator had two accelerometers mounted at their tips near the leading and trailing edges. The strain gages were attached to the attachment stubs of the two vertical fins and the temperature sensor attached the surface of the left vertical fin. Data was sampled at a rate of 512 Hz per channel for a period of 32 seconds. To eliminate concerns for frequency damping due to pressure lines and to ease transducer installation, absolute pressure transducers, that did not have reference pressure lines, were installed on the tail surface. Fairings, depicted in Fig. 6, were mounted around each pressure transducer to eliminate pressure disturbances due to the transducers obstructing the flow. The signals from the pressure transducers were A/C coupled to eliminate the large D/C

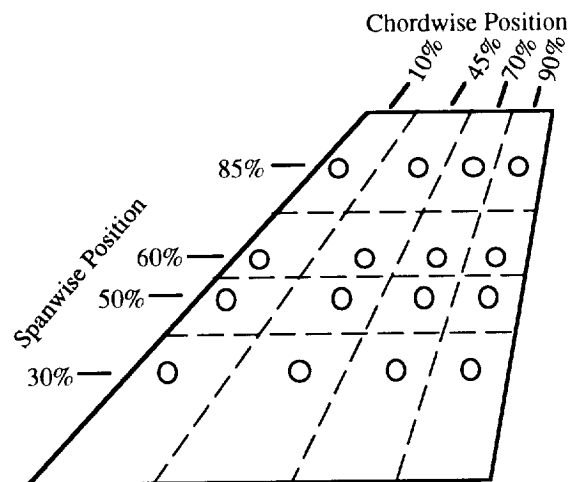


Fig. 5 Pressure transducer locations, left vertical fin.

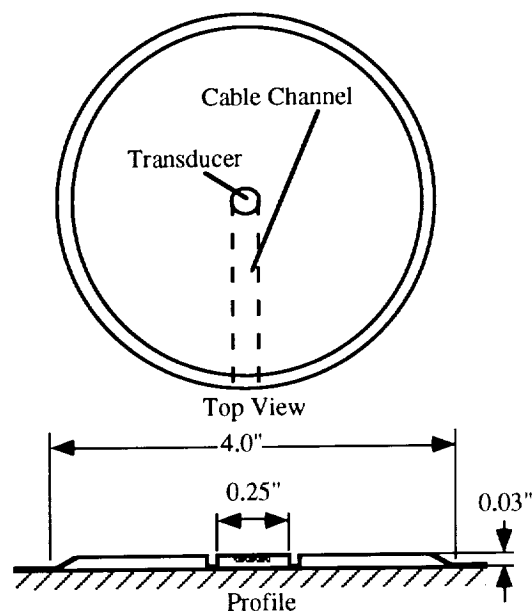


Fig. 6 Pressure transducer fairing.

offset due to atmospheric pressure and thereby allowing greater signal gain for increased resolution of the unsteady pressures measured.

Ground Vibration Tests

Ground vibration tests were conducted on the aircraft and on the vertical fins in particular to determine if the bending modes and natural frequencies were affected by the lack of engines and by mounting the aircraft on struts. These tests were conducted by a team from the U.S. Air Force's Wright Research Laboratory¹⁰. Ground vibration tests were performed on the aircraft both on the ground and mounted on the wind tunnel struts. The vertical fin had first structural bending mode at 15 Hz, second bending mode at 62 Hz, and first torsion mode at 44 Hz; these values are very close to those of a fully configured production aircraft.

Test Conditions

Most of the test was conducted at a free stream velocity of 168 ft/s. This corresponds to a dynamic pressure of 33 psf, a Mach number of 0.15, and a Reynolds number of 12.3×10^6 based on mean aerodynamic chord. The lowest velocity tested was 65 ft/s, which corresponds to a dynamic pressure of 5 psf. The angle-of-attack ranged from 18° to 50° and the angle-of-sideslip ranged from -15° to 15° . Only data from the zero sideslip condition is presented in this paper.

ANALYSIS METHODS

Data Reduction

The method chosen to estimate the power spectral distribution (PSD) was a single-sided periodogram utilizing a Fast-Fourier-Transform algorithm. This is a classical method of PSD estimation, and it has the advantage that the integral of the estimated PSD with respect to frequency is equal to the variance (or the RMS^2) of the signal. To determine a time-averaged PSD, the 32 second time record, which contained 16384 samples, was subdivided into 127 half-second time records that overlapped by 50%. A Hann window was applied to each record, which contained 256 samples, and then each record was padded with zeros to increase the record length to 4096. PSDs were calculated for each record and averaged to yield a time-averaged PSD.

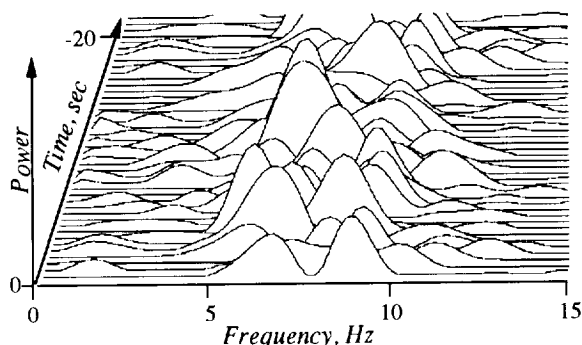


Fig. 7 Typical time-frequency plot of differential pressure on the vertical tail.

This method of data reduction was chosen due to the chaotic nature of tail buffet pressures. The variation of the PSDs with time for any signal is quite significant, as can be seen in Fig. 7, which shows PSDs at half-second intervals for a differential pressure on the vertical tail. Such a signal is said to have "noise-like" properties and time-averaging is required to reduce error in the PSD estimates. The difference that time averaging makes is very dramatic. Figure 8 shows the estimated PSD when the entire record of 16384 samples is used. This PSD has a frequency resolution of 0.031 Hz, but the estimated standard deviation for a non-averaged PSD is 100%. Averaging reduces the standard deviation by the square-root of the number of averages, so the PSD estimate shown by the solid line in Fig. 9, which is based on 127 half-second PSDs, has an estimated standard deviation of less than 9%. Unfortunately, the frequency resolution for

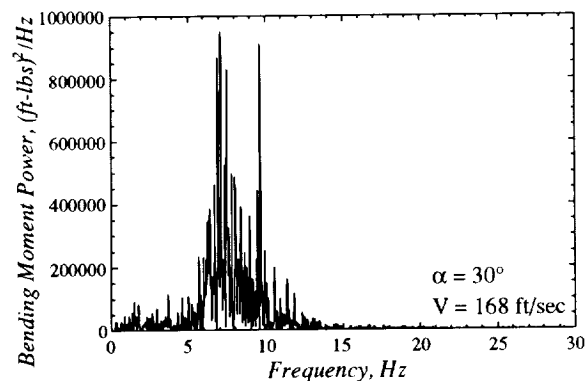


Fig. 8 Typical full record power spectrum.

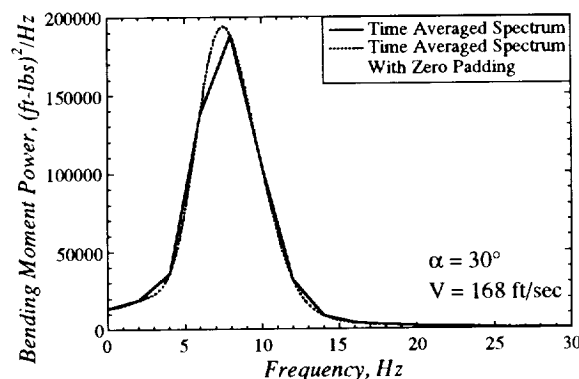


Fig. 9 Typical time-averaged power spectra, with and without zero padding.

this PSD is only 2 Hz. To regain some of the frequency resolution lost by using half-second time records, enough zeros are added to each record to increase the time period to 8 seconds. The effect of zero padding is shown by the dashed line in Fig. 9, which has an effective frequency resolution of 0.125 Hz. Although zero padding increases the effective resolution for distributed power, in this case, it can not resolve single-frequency tones that are separated by less than 2 Hz. However, since the tail buffet pressure signals do not seem to contain persistent, single-frequency tones, zero padding is a reasonable means of increasing the effective resolution of the time-averaged PSDs.

Differential pressures were calculated by subtracting the inboard pressure value from the corresponding outboard pressure for each time step. To calculate bending moments due to buffet pressure, the surface area of the vertical fin was divided as shown in Fig. 5. The differential pressures measured at the transducer locations shown were multiplied by the area of the enclosing sub-section and by the distance of the sub-section centroid from the fin root. These values for all 16 sub-sections were then summed for each time step to obtain a time history for the bending moment imposed by the pressure field on the fin.

Non-Dimensional Parameters

The derivations of non-dimensional parameters for frequency, Root-Mean-Square (RMS) pressure, and buffet pressure PSDs are given in reference 1. The definitions

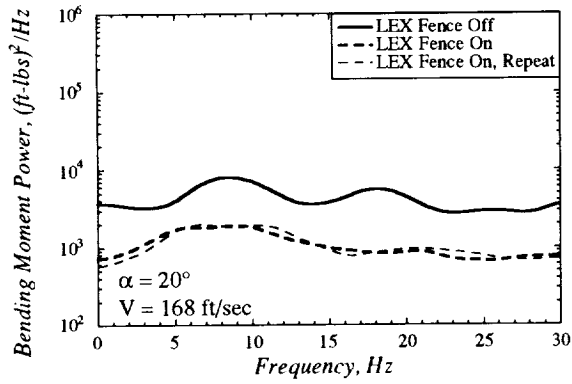


Fig. 10(a).

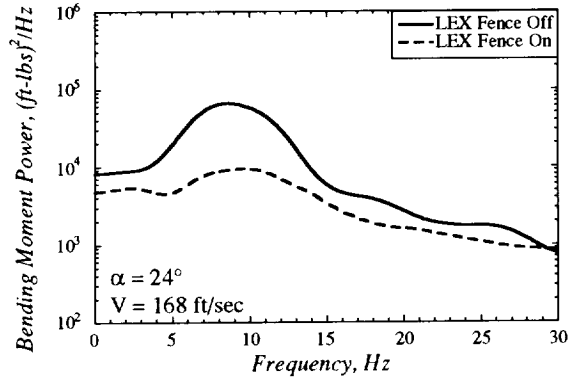


Fig. 10(b).

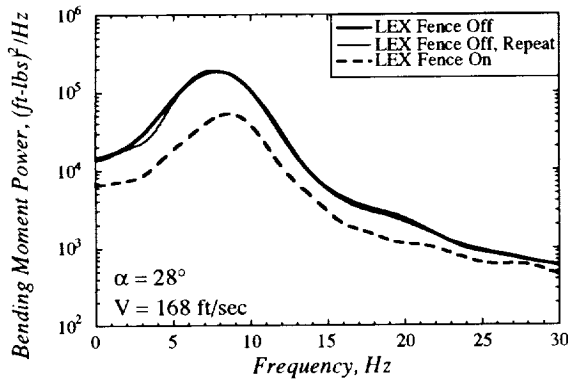


Fig. 10(c).

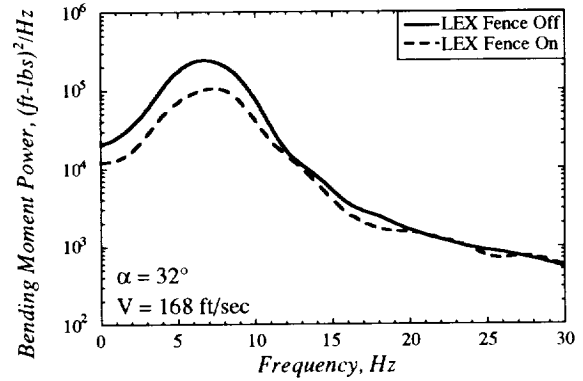


Fig. 10(d).

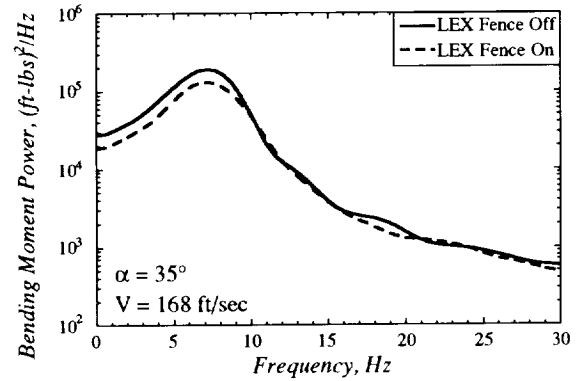


Fig. 10(e).

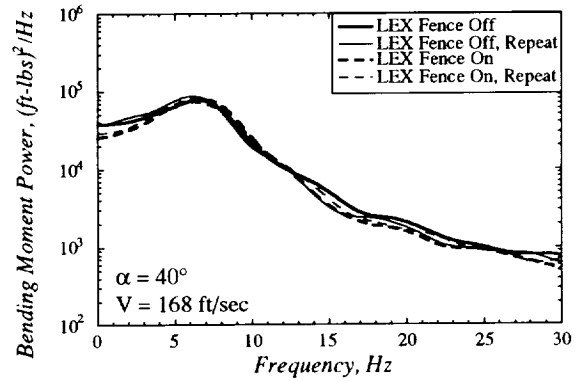


Fig. 10(f).

Fig. 10 Bending moment power spectra for $\alpha = 20^\circ$ to 40° . Both with and without the LEX fence.

for the reduced frequency, F , the RMS pressure coefficient, C'_p , and the pressure PSD coefficient, C''_p , are given in the nomenclature. For this paper the mean aerodynamic chord (11.52 ft) was chosen as the length scale, l , and the free stream velocity was chosen as the characteristic velocity, V .

EXPERIMENTAL RESULTS

LEX Fence Effect

Figure 10 shows bending moment power spectra for the port-side vertical tail for angles-of-attack from 20° to 40° . The data repeatability is demonstrated in Figs. 10 (a, c, and f). As shown, the LEX fence is an effective means

of reducing the bending moment power up to an angle-of-attack of 32° . Flow visualizations that were conducted during the test indicated that the LEX vortex bursts well ahead of the LEX fence position for angles-of-attack greater than 35° . For these angles-of-attack, the buffeting that occurs is most likely due to the wake of the wing and fuselage. The LEX fence retains some effectiveness at 35° , Fig. 10(e); however, there is no LEX fence effect at 40° , Fig. 10(f). Although the data is not presented here, there is no LEX fence effect at 45° and 50° angle-of-attack.

Figure 11 shows the variation in RMS bending moment with angle-of-attack. The LEX fence reduces the

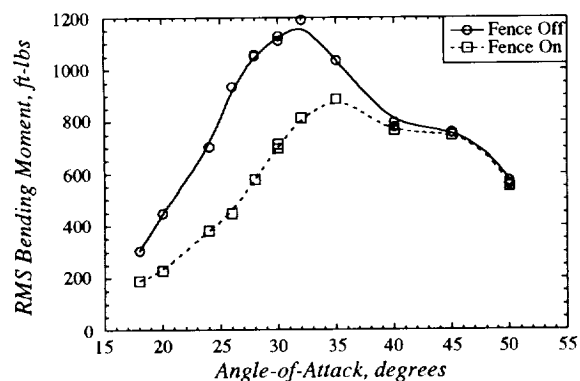


Fig. 11 Variation of RMS bending moment with angle-of-attack.

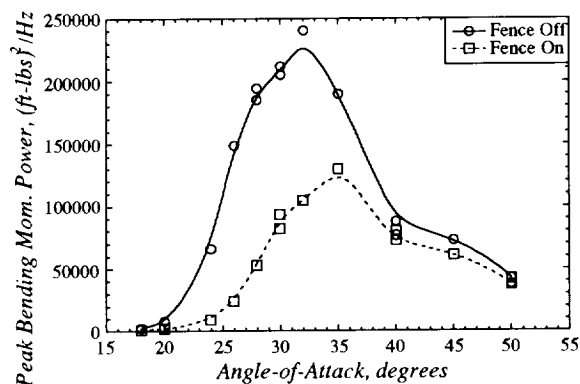


Fig. 12 Variation of peak bending moment power with angle-of-attack.

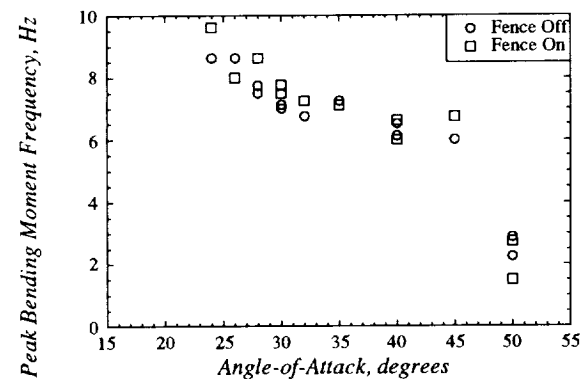


Fig. 13 Variation of peak bending moment frequency with angle-of-attack.

variation in the peak power with angle-of-attack for the time-averaged bending moment power spectra. The LEX fence reduces peak power for angles-of-attack less than 40° and the magnitude of the maximum peak power attained is reduced by nearly 50%. The frequency of the peak power, shown in Fig. 13, is not significantly affected by the LEX fence. Frequency data is not shown for angles-of-attack less than 24° because, the power spectra did not contain clearly defined and repeatable peaks.

Scale Effects

Small-scale tests have shown that tail buffet power spectra scale very well with velocity.¹ This is also true for the full-scale test. Figure 14 presents the non-

dimensional PSDs for the pressure transducer at the 60% span, 45% chord, inboard location for velocities of 168 ft/sec and 130 ft/sec. The excellent agreement exhibited over the entire frequency range indicates that velocity scaling is valid at full-scale test conditions.

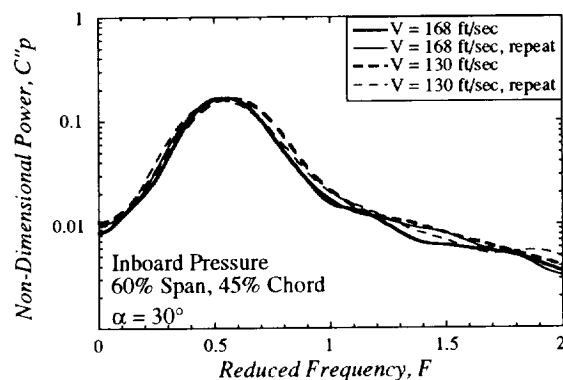


Fig. 14 Non-dimensional power spectra for two velocities.

The comparisons of full- with small-scale data presented in this paper are for the 60% span and 45% chord location. First, comparisons between full- and 12%-scale¹ differential pressure data are presented. Then, comparisons between full-, 16%-³, and 6%-scale⁵ inboard and outboard pressure data are presented. Data for both the LEX fence off and on are presented where available.

Figure 15 shows comparisons of non-dimensional power spectra from the full- and 12%-scale tests for angles-of-attack from 24° to 36°. Full-scale data was not available for 36°, so data for 35° is shown. The power spectra for 24°, 28°, and 32°, Figs. 15(a,b, and c) show good agreement for frequencies at and above the peak in the PSD, but the full-scale power spectra have more power in the lower frequencies. The comparison between the power spectra for 35° and 36°, Fig. 15(d), shows that the peak power for the 12%-scale is significantly greater than that for the full-scale. This indicates something unusual may have occurred at 36° angle-of-attack on the small-scale model, that did not occur for the full-scale test.

Figure 16 shows the reduced frequency of the peaks in the differential pressure power spectra, for the full-scale and 12%-scale. The full-scale frequency is in good agreement with the 12%-scale frequency up to 45° angle-of-attack. At 50°, the full-scale frequency drops below the frequencies shown for the 12%-scale model at 48° and 52° angle-of-attack. The LEX fence, at full-scale, is shown to have negligible effect on reduced frequency.

Figure 17 shows that the full-scale RMS pressure coefficients are noticeably higher than those of the 12%-scale at angles-of-attack less than 35°. At 35° angle-of-attack and greater the full-scale and 12%-scale RMS pressure coefficients are in very good agreement. The LEX fence, at full-scale, is shown to reduce the differential RMS pressure at 35° angle-of-attack and lower.

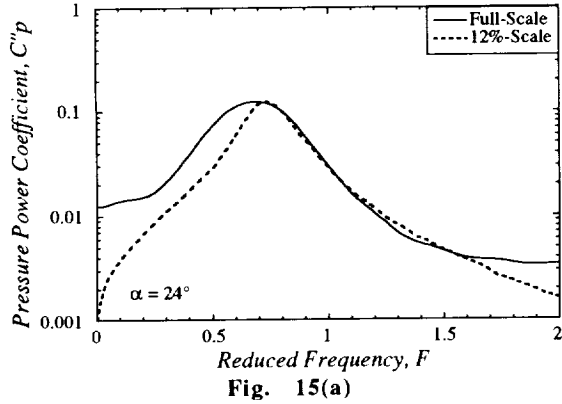


Fig. 15(a)

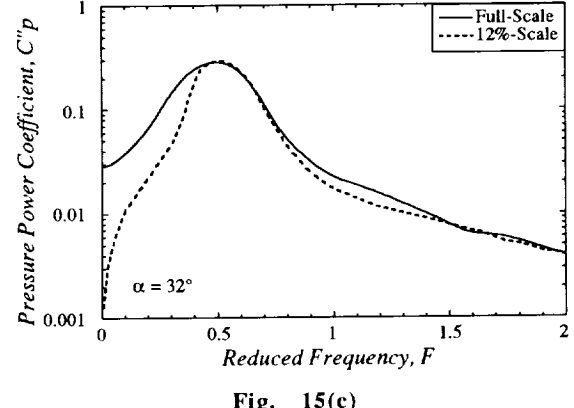


Fig. 15(c)

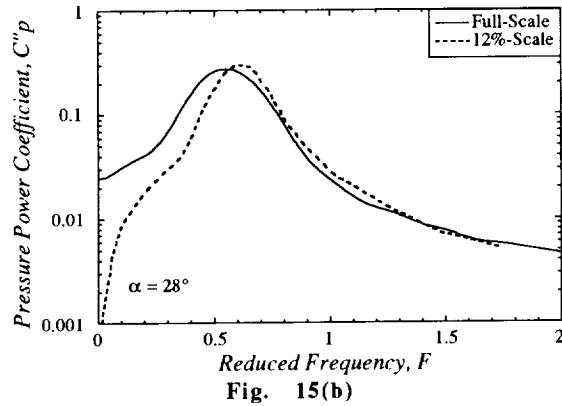


Fig. 15(b)

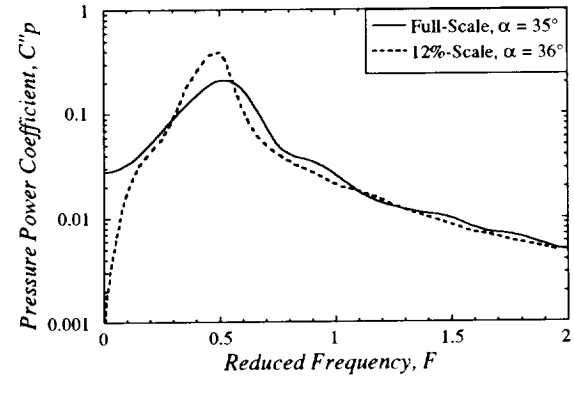


Fig. 15(d)

Fig. 15 Differential pressure power at 60%-span and 45%-chord on the vertical tail of the full-scale and 12%-scale models. (a) $\alpha = 24^\circ$, (b) $\alpha = 28^\circ$, (c) $\alpha = 32^\circ$, and (d) $\alpha = 35^\circ$ full-scale / $\alpha = 36^\circ$ 12%-scale.

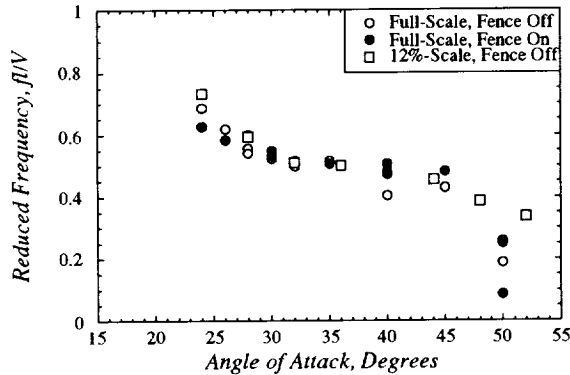


Fig. 16 Non-dimensional peak power frequency for differential pressure at 60%-span and 45%-chord on the vertical tail.

The peak differential PSD pressure coefficient is shown in Fig. 18 as a function of angle-of-attack. The coefficients agree remarkably well for full-scale and 12%-scale, except for the 12%-scale points at 36° and 44° angle-of-attack. The full-scale data shows a relatively smooth variation in peak power with angle-of-attack and the peak power decreases for angles-of-attack greater than 32° . The 12%-scale data shows the peak power leveling off around 28° and 32° angle-of-attack and then jumping abruptly for 36° . This indicates that something unusual

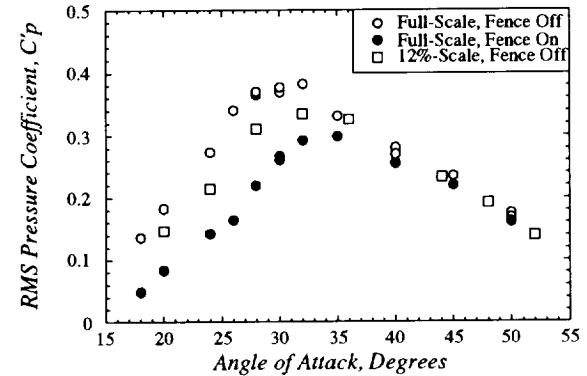


Fig. 17 RMS pressure coefficient for differential pressure at 60%-span and 45%-chord on the vertical tail.

is happening around 36° angle-of-attack for the 12%-scale, that does not occur at full-scale. The LEX fence, at full-scale, is shown to significantly reduce the peak differential PSD pressure at 35° angle-of-attack and lower. The overall maximum differential PSD pressure is reduced by 50% with the LEX fence on.

Comparisons of full-scale inboard and outboard pressure data with 16%- and 6%-scale data are shown in Figs. 19 and 20. Figure 19(a) shows the reduced frequency of the peaks in the inboard pressure power

spectra and Fig. 19(b) shows the reduced frequency for the outboard pressure. The full-scale data in both figures

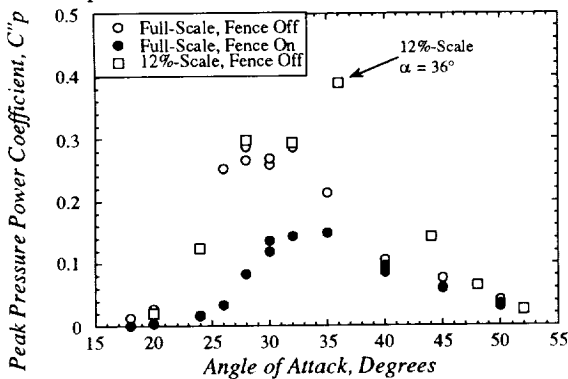


Fig. 18 Peak pressure power coefficient for differential pressure at 60%-span and 45%-chord on the vertical tail.

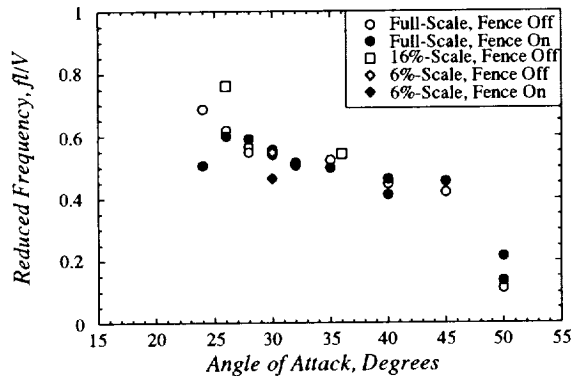


Fig. 19(a) Non-dimensional peak power frequency for inboard pressure at 60%-span and 45%-chord on the vertical tail.

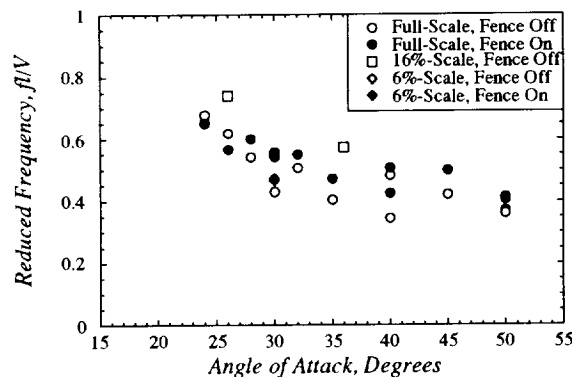


Fig. 19(b) Non-dimensional peak power frequency for outboard pressure at 60%-span and 45%-chord on the vertical tail.

exhibits more scatter than was shown for the frequencies found for differential pressure, Fig. 16. The large amount of scatter makes it difficult to draw any clear conclusions from the data presented in Fig. 19. However, the 16%-scale frequencies are consistently higher than the full- and 6%-scale frequencies in both Figs. 19(a) and 19(b).

Figure 20(a) shows the RMS pressure coefficient for inboard pressure data. The full-scale RMS pressure coefficient is consistently greater than small-scale for

angles-of-attack less than 36°. At 36°, the 16%-scale has a slightly higher RMS pressure coefficient. The effect of the LEX fence at all three scales is to reduce the RMS pressure for angles-of-attack of 36° and less. The outboard RMS pressure coefficients, Fig. 20(b), are lower than the inboard RMS pressures in the angle-of-attack range from 24° to 45°. The scatter in the data shown in Fig 20(b), makes it difficult to draw any clear conclusions about the differences between model scales or about the effect of the LEX fence. Overall the inboard pressure would seem to contribute more to tail buffet loads than does the outboard pressure.

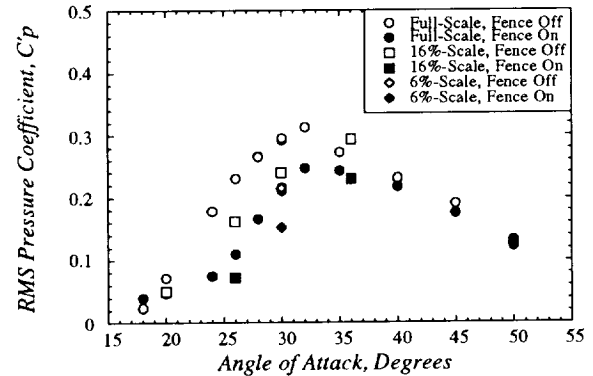


Fig. 20(a) RMS pressure coefficient for inboard pressure at 60%-span and 45%-chord on the vertical tail.

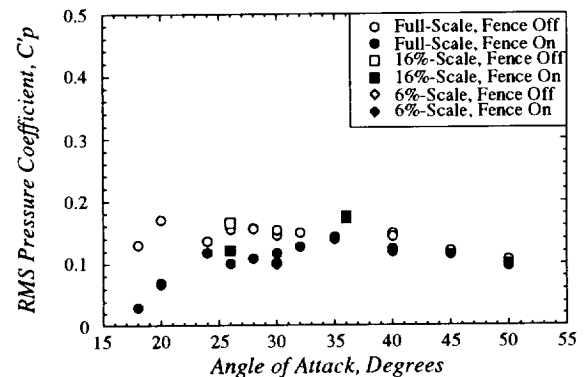


Fig. 20(b) RMS pressure coefficient for outboard pressure at 60%-span and 45%-chord on the vertical tail.

CONCLUDING REMARKS

The LEX fence significantly reduces RMS bending moment and peak PSD bending moment. It also significantly reduces RMS pressure and peak PSD pressure at all model-scales. The LEX fence did not significantly affect the peak power frequency.

Non-dimensional peak power frequencies measured in small-scale tests agree well with the full-scale frequencies. However, non-dimensional RMS pressures measured on the full-scale aircraft were greater than those measured in small-scale tests for angles-of-attack less than 40°. Comparisons of the non-dimensional power spectra for the full-scale aircraft and the 12%-scale model show that the full-scale power spectra have more power in the frequencies below the peak power frequency. Above this

frequency, the non-dimensional power spectra for both model scales are in good agreement.

REFERENCES

- 1 Zimmerman, N.H. and Ferman, M.A.: "Prediction of Tail Buffet Loads for Design Application," NADC-88043-60, July 1987.
- 2 Martin, C.A.; Glaister, M.K.; MacLaren, L.D.; Meyn, L.A.; and Ross, J.: "F/A-18 1/9th Scale Model Tail Buffet Measurements," Flight Mechanics Report 188, Aeronautical Research Laboratory, Melbourne Australia, June 1991.
- 3 Shah, G.H.: "Wind-Tunnel Investigation of Aerodynamic and Tail Buffet Characteristics of Leading-Edge Extension Modifications to the F/A-18," AIAA Paper 91-2889, Atmospheric Flight Mechanics Conference, August 1991.
- 4 Shah, G.H.; Grafton, S.B.; Gynn, M.D.; Brandon, J.M.; Dansberry, B.E.; and Patel, S.R.: "Effect of Vortex Flow Characteristics on Tail Buffet and High-Angle-of-Attack Aerodynamics of a Twin-Tail Fighter Configuration," High-Angle-of-Attack Technology Conference, October 1990.
- 5 Lee, B.H.K. and Brown, D.: "Wind-Tunnel Studies of F/A-18 Tail Buffet," Journal of Aircraft, Vol. 29, No. 1, 1992, pp. 146-152.
- 6 Rizk, Y.M. and Gee, K.: "Numerical Prediction Of The Unsteady Flowfield Around The F-18 Aircraft At Large Incidence," AIAA Paper 91-0020, 29th Aerospace Sciences Meeting, January 1991.
- 7 Rizk, Y.M.; Guruswamy, G.P.; and Gee, K.: "Computational Study of F-18 Vortex Induced Tail Buffet," AIAA Paper 992-4699, 4th Symposium on Multidisciplinary Analysis and Optimization, September 1992.
- 8 Meyn, L.A.; Lanser, W.R.; and James, K.D.: "Full-Scale High Angle-of-Attack Tests of an F/A-18," AIAA Paper 92-2676, 10th Applied Aerodynamics Conference, June 1992.
- 9 Corsiglia, V.R.; Olson, L.E.; and Falarski, M.D.: "Aerodynamic Characteristics of the 40- by 80/80- by 120-Foot Wind Tunnel at NASA Ames Research Center," NASA TM 85946, April 1984.
- 10 Levraea, V.J.; Henderson, D.A.; Pacia, A.P.; Banford, M.P.: "Modal Survey of a Full-Scale F-18 Wind Tunnel Model," Wright Laboratory, WL-TM-92-350-FIBG, September 1992.